Comparing multiparticle production within a two-component dual parton model with collider data

K. Hahn and J. Ranft
Sektion Physik, Karl-Marx-Universität, Leipzig, German Democratic Republic
(Received 17 July 1989)

The dual parton model (DPM) is very successful in describing hadronic multiparticle production. The version of DPM presented includes both soft and hard mechanisms. The hard component is described according to the lowest-order perturbative QCD–parton-model cross section. The model is formulated in the form of a Monte Carlo event generator. Results obtained with this event generator are compared with data on inclusive reactions in the TeV energy range of the CERN and Fermilab hadron colliders.

I. INTRODUCTION

Since the beginning of the 1980s several groups have studied soft hadronic multiparticle production in the framework of the dual topological unitarization (DTU) model. This model and in particular the Monte Carlo formulation of this model in the form of the dual multichain fragmentation model[1–5] provide one of the starting points for the new model described here.

Experimental observations made it clear that at collider energies the soft and hard components of hadronic multiparticle production are closely related. These observations are the discovery, at the CERN Super Proton Synchrotron collider, of correlations between the average transverse momenta of hadrons produced and the multiplicity density in rapidity[6] and the observation of "minijets" in hadronic collisions and changes of the properties of the underlying soft events in data samples with jets or minijets.[7]

These properties were understood within the dual multichain fragmentation model[5] by introducing transverse momenta (in addition to intrinsic transverse momenta) with magnitudes, which could only be interpreted as due to hard constituent scattering for the partons at the ends of the fragmenting chains.

The perturbative hard constituent scatterings are also one of the processes responsible for the rise of the hadronic cross sections. This was studied quantitatively by Capella, Tran Thanh Van, and Kwiecinski[8] and by Durand and Pi,[9], where the consequences for the total and inelastic cross sections of the unitarization of soft- and hard-scattering cross sections were studied. This model, as formulated by Capella *et al.*,[8] is the second starting point for the model to be described here.

A first description of the model as well as comparisons to experimental data and predictions for the energy $\sqrt{s}=40$ TeV of the Superconducting Super Collider were given by Ranft *et al.*[10] The model is implemented in the form of the Monte Carlo code DTUJET.[11,12] There are other Monte Carlo implementations of the dual parton model (DPM) and related models for hadron-hadron, hadron-nucleus, and nucleus-nucleus collisions[13–17] which successfully describe many features of the experimental data. DTUJET is the only code implementing the unitarized hard and soft components according to the scheme.[8,9]

In the present paper we concentrate on the sampling of hard jets and minijets via a Monte Carlo algorithm and give for completeness a short description of the unitarization scheme and of the other parts of the model.

The two-component dual parton model, which includes soft and hard components, is discussed in Sec. II. In Sec. III we describe the hard component and the Monte Carlo algorithm to sample hard-scattering events. Some more technical things are explained in the Appendix. Section IV contains the results and the comparison with experimental data.

II. THE TWO-COMPONENT DUAL PARTON MODEL

In this section we will discuss the basic ideas of the dual parton model and the way in which the hard component is included. For a more complete description we refer to Refs. 8 and 10.

At higher energies the hadron-hadron interaction is dominated by Pomeron exchange. The Pomeron is cut into two chains (or strings) and these chains are connected to the hadron constituents. In the leading order the proton consists of one valence quark and one valence diquark and the interaction between the hadrons results from the chains which are stretched between these constituents. Figure 1(a) shows the leading diagram (one cut Pomeron) for a pure soft p-$\bar{p}$ collision.

The Pomeron exchange corresponds to a pure soft cross section and can be parametrized[8] as

$$\sigma_s = a s^{\alpha-1} \tag{2.1}$$

with $a=37.8$ mb and $\alpha=1.076$. This cross section increases with energy and violates the unitarity bound at higher energies. The same applies to the pure hard-scattering cross section σ_h. In Fig. 2 we give the total, inelastic, and hard cross sections as a function of the center-of-mass energy $\sqrt{s}$. The hard cross section is calculated with a lower transverse-momentum cut $p_{\perp,\min}=2$

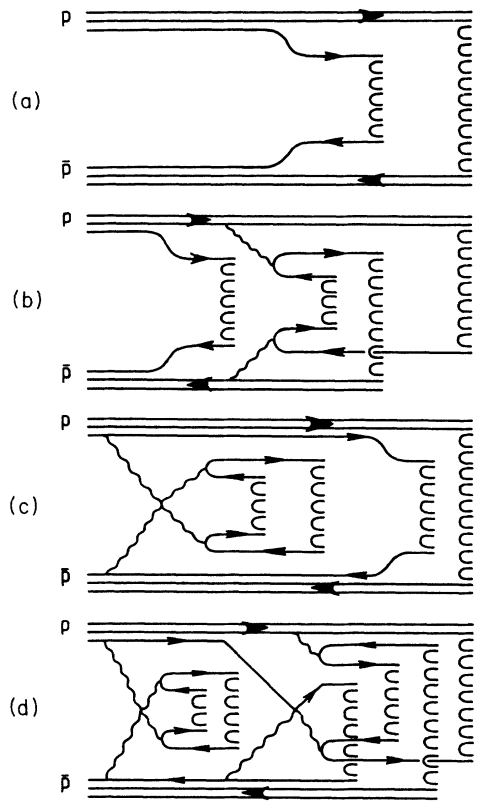

FIG. 1. Diagrams for the exchange of soft and hard chains; (a) one soft cut Pomeron (two soft chains), (b) two soft cut Pomerons (four chains), (c) one soft and one hard cut Pomeron (two soft, two hard chains), (d) one soft and two hard cut Pomerons.

GeV/c. The hard cross section increases with energy $\sqrt{s}$ practically as a power of s whereas the total cross section is proportional to $(\ln s)^2$ so that it exceeds the total cross section $\sigma_{\rm tot}$ at higher energies. Both the hard cross section σ_h and the pure soft cross section σ_s are inclusive cross sections and the average multiplicities of hard and soft scatterings in an inelastic event are $\langle n_h \rangle = \sigma_h/\sigma_{\rm inel}$ and $\langle n_s \rangle = \sigma_s/\sigma_{\rm inel}$, respectively. These multiplicities increase with energy and at higher $\sqrt{s}$ a sizable part of the events has more than one hard or soft scattering. The multiplicities are calculated with a unitarization scheme[8] which is a generalization of the Abramouski-Gribov-Kancheli (AGK) cutting rules.[18] This scheme gives the weights for events with i soft and j hard scatterings.[10]

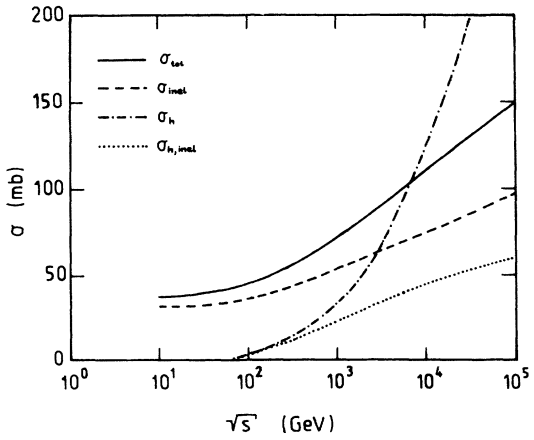

FIG. 2. Total, inelastic, and hard cross sections as functions of energy $\sqrt{s}$ as obtained from the model.

A next-to-leading-order diagram (two cut Pomerons) is given in Fig. 1(b). Here the hadron constituents are also sea quarks and cutting the Pomeron we get chains with the sea quarks at the ends.

In Fig. 1(c) we give an example how a hard component is added to the leading pure soft diagram. Here two gluons undergo a hard $2\rightarrow 2$ scattering and the resulting gluons which have transverse momenta $p_\perp \geq p_{\perp,\min}$ are split into quark-antiquark pairs. These quarks and antiquarks sit at the ends of further chains.

An example for an event with two hard and one soft scatterings is given in Fig. 1(d). The hard scatterings are mostly independent of each other and the only interconnection is the sharing of energy and momentum of the incoming hadrons. The number of hard jets and minijets in an event is two times the number of hard scatterings and so the average jet multiplicity should increase with energy due to increasing $\langle n_h \rangle$.

III. THE HARD SCATTERING

A. The total hard cross section

The QCD–parton-model formula for hard scattering is

$$\sigma_h = \sum_{i,j\rightarrow k,l} \int\int\int dx_1 dx_2 d\hat{t}\, x_1 f_i(x_1,Q^2) \times x_2 f_i(x_2,Q^2) \frac{1}{x_1 x_2} \pi M^2 \frac{\alpha_s^2(Q^2)}{\hat{s}^2}\ , \tag{3.1}$$

where $f_{i,j}(x_{1,2},Q^2)$ are the parton distributions, $M = M_{i,j\rightarrow k,l}$ is the matrix element for the hard parton-parton scattering, $i+j\rightarrow k+l$, $\alpha_s(Q^2) = 4\pi/b_0 \ln(Q^2/\Lambda^2)$ is the strong coupling constant, $b_0 = 11 - \frac{2}{3}n_f$, and n_f is the number of flavors.

The hard-scattering cross section (3.1) depends strongly on the lower transverse-momentum cut $p_{\perp,\min}$ which has to be introduced to remain in the region where the perturbation theory is valid. In Fig. 3 we present σ_h as a function of $p_{\perp,\min}$ for $\sqrt{s} = 200$ and 1800 GeV. The value which we use in our calculations is $p_{\perp,\min} = 2$ GeV/c. This choice should avoid another problem; the dense packing of partons.[19] At small x the number of partons grows rapidly and will reach a point where the partons no longer behave as free particles and recombinations become important, so that the Altarelli-Parisi evolution of parton distributions becomes invalid. A $p_\perp$ cut of 2 GeV/c should avoid this problem[20] up to the energy $\sqrt{s} = 40$ TeV of the proposed Superconducting Super Collider. But even if the Altarelli-Parisi equations are valid, the parton distributions are not well determined. These equations need, as input, the parton distributions at a fixed Q_0^2, and evolve these distributions to higher

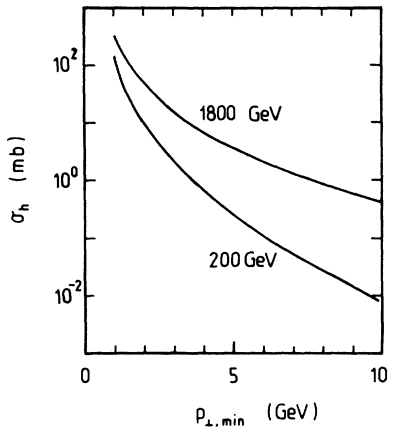

FIG. 3. The hard cross section σ_h as a function of $p_{\perp,\min}$ for $\sqrt{s}=200$ and 1800 GeV.

values of Q^2. Because experimental data are not available for small x at Q_0^2, an extrapolation is needed and usually a $1/x$ behavior of the sea quark and gluon distributions is assumed. There are arguments[21] that favor a $1/x^a$ behavior with $a=1.3-1.5$. We have implemented in our Monte Carlo event generator DTUJET parton distributions which assume a $1/x$ behavior [Eichten-Hinchliffe-Lane-Quigg[22] (EHLQ) sets 1 and 2 and Martin-Roberts-Sterling[23] (MRS) sets 1 and 2] and one parametrization with a $1/x^{1.5}$ behavior (MRS[23] set 3). A comparison (Fig. 4) of the total hard cross sections σ_h calculated with these parametrizations shows no striking differences, except for MRS[23] set 3, which results in a σ_h exceeding the others by an order of magnitude for higher energies. We use for all calculations set 1 from Martin *et al.*[23]

The choice of the hard scale Q^2 in $\alpha_s(Q^2)$ and $f(x,Q^2)$ is also not well determined and can only be fixed by the inclusion of higher-order terms, but these are neglected here. Different alternatives such as $Q^2=\hat{s}$ or $Q^2=p_\perp^2$ are possible and we use $Q^2=p_\perp^2/4$ both for $\alpha_s(Q^2)$ and $f(x,Q^2)$. Because of the freedom in Q^2, one can expect uncertainties in the hard cross section of about 20%.

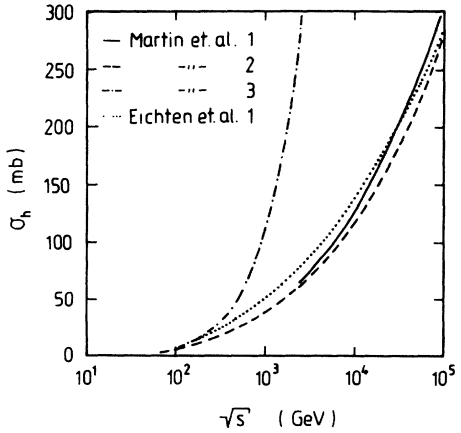

FIG. 4. The hard cross section σ_h as a function of energy for different parton distributions (Refs. 22 and 23).

The QCD scale parameter Λ in $\alpha_s(Q^2)$ is taken according to the used parton distributions. The corresponding values of Λ are the following: EHLQ set 1, $\Lambda=0.2$ GeV; EHLQ set 2, $\Lambda=0.29$ GeV; MRS set 1, $\Lambda=0.107$ GeV; MRS set 2, $\Lambda=0.25$ GeV; and MRS set 3, $\Lambda=0.178$ GeV.

B. Kinematics

In this section we give a short collection of kinematical relations and introduce some new variables.

To write down the matrix elements M_m^2 we introduce new variables

$$v=\frac{\hat{t}}{\hat{s}}\ ,\qquad u=\frac{\hat{u}}{\hat{s}}\ , \tag{3.2}$$

for the parton-parton scattering instead of the commonly used Mandelstam variables $\hat{t}$ and $\hat{u}$. The matrix elements in Table I are given in terms of these new variables. u and v are not independent but are related by

$$1+u+v=0\ . \tag{3.3}$$

The variables which are used in the Monte Carlo algorithm are x_1, x_2, and $v=\hat{t}/\hat{s}$. The quantities transverse momentum $p_\perp$ and pseudorapidity η_k and η_l of the final partons are related to x_1, x_2, and v as

$$p_\perp^2=-\hat{t}\left[\frac{\hat{t}}{s}+1\right]=uv\hat{s}\ ,$$
$$\eta_k=\tfrac{1}{2}\ln\left[\frac{ux_1}{vx_2}\right]\ , \tag{3.4}$$
$$\eta_l=\tfrac{1}{2}\ln\left[\frac{vx_1}{ux_2}\right]\ ,$$

TABLE I. Matrix elements M_m, symmetry factors S_m, and final-state summation factors N_m for the hard subprocesses.

Process	M_m^2	S_m	N_m
$gg\to gg$	$\frac{9}{2}\left[3-uv-\frac{u}{v^2}-\frac{v}{u^2}\right]$	$\frac{1}{2}$	
$q\bar{q}\to gg$	$\frac{32}{27}\frac{u^2+v^2}{uv}-\frac{8}{3}(u^2+v^2)$	$\frac{1}{2}$	
$gq\to gq$	$\frac{1+u^2}{v^2}-\frac{4}{9}\frac{1+u^2}{u}$		
$gg\to q\bar{q}$	$\frac{1}{6}\frac{u^2+v^2}{uv}-\frac{3}{8}(u^2+v^2)$		n_f
$q\bar{q}\to q\bar{q}$	$\frac{4}{9}\left[\frac{1+u^2}{v^2}+u^2+v^2\right]-\frac{8}{27}\frac{u^2}{v}$		
$q\bar{q}\to q'\bar{q}'$	$\frac{4}{9}(u^2+v^2)$		n_f-1
$qq\to qq$	$\frac{4}{9}\left[\frac{1+u^2}{v^2}+\frac{1+v^2}{u^2}\right]-\frac{8}{27}\frac{1}{uv}$	$\frac{1}{2}$	
$qq'\to qq'$	$\frac{4}{9}\frac{1+u^2}{v^2}$		

where $u=-(1+v)=\hat{u}/\hat{s}$.

Up to now we have not given the integration ranges in (3.1). These ranges are

$$a \le x_1 \le 1 ,$$

$$a \le x_2 \le 1 , \tag{3.5}$$

$$-\tfrac{1}{2}(1+W) \le v \le -\tfrac{1}{2}(1-W) ,$$

with

$$a=\frac{4p_{\perp,\min}^2}{s}, \quad W=\left[1-\frac{a}{x_1x_2}\right]^{1/2} .$$

Additionally one has to introduce an extra term $\Theta(x_1x_2-a)$ into the integrand of (3.1).

C. The Monte Carlo algorithm for hard scatterings

The sampling of hard parton-parton scattering is already implemented in codes such as ISAJET (Ref. 24) and PYTHIA.[25] We use here a modified algorithm. Formula (3.1) is used to sample the kinematical variables, subprocess types, and parton types for the hard scattering. To do this in a numerically efficient way some reorderings and transformations are necessary.

The sum $\sum_{i,j\to k,l}$ in (3.1) runs over all possible parton configurations; i.e., the indices i and j run over gluon and all quark flavors and k and l run over all possible final configurations for i and j given. For use in our algorithm, we reorder the sum in such a way that first it is summed over all subprocesses (e.g., $g+g\to g+g$, $q+g\to q+g$, $q+\bar{q}\to q+\bar{q}$, etc.) and then it is summed over the remaining configurations that are possible for the given subprocess. Because all partons are assumed to be massless, we can replace the sum over the final states k,l by a simple factor N_m denoting the number of final states for subprocess m and initial partons i,j given. These factors, the symmetry factors coming from identical particles in the final state, and the matrix elements[26] for the eight hard pure hadronic subprocesses are given in Table I.

Cross section (3.1) with the reordered sum and the new variables becomes

$$\sigma_h=\sum_m N_m \sum_{i,j}^{(m)} \int\int\int dx_1dx_2dv\, x_1f_i(x_1,Q^2)x_2 f_j(x_2,Q^2)\frac{1}{x_1x_2}\pi M_m^2\frac{\alpha_s^2(Q^2)}{\hat{s}} \times\Theta(x_1x_2-a) , \tag{3.6}$$

where $\sum_{i,j}^{(m)}$ means that i and j are restricted to subprocess m.

A direct sampling of x_1, x_2, and v from the integrand of (3.6) would be inefficient due to the strong rise at small x and at the borders of the v range. To get a more efficient algorithm we split the integrand into two parts:

$$g_m(x_1,x_2,v)=\frac{\pi}{s}M_m^2\frac{1}{(x_1x_2)^2}\Theta(x_1x_2-a) ,$$

$$h_m(x_1,x_2,v)=\sum_{i,j}^{(m)} x_1f_i(x_1,Q^2)x_2f_j(x_2,Q^2)\alpha_s^2(Q^2) .$$

g_m is relatively simple, in the sense that it contains no complicated functions. The singularity structure is clearly visible and sampling of x_1, x_2, and v from the distribution $g(x_1,x_2,v)dx_1dx_2dv$ is straightforward. h_m contains the more complicated functions, but depends only weakly on x_1, x_2, and v. h_m is used as weight to accept or reject the set x_1,x_2,v as chosen from g_m.

Then one can rewrite (3.1) as

$$\sigma_h=\sum_m\int\int\int dx_1dx_2dv\, g_mh_m , =\sum_m\int_0^1\int_0^1\int_0^1 d\xi_1d\xi_2d\xi_3\hat{h}_m , \tag{3.7}$$

where

$$\hat{h}_m=A_mh_m$$

and

$$A_m=\int_a^1\int_a^1\int_{-0.5(1+W)}^{-0.5(1-W)}dx_1dx_2dv\, g_m(x_1,x_2,v) .$$

The new variables ξ_i are related to x_1, x_2, and v,

$$d\xi_1d\xi_2d\xi_3=\frac{g_m(x_1,x_2,v)}{A_m}dx_1dx_2dv ,$$

which means that x_1, x_2, and v are sampled from the distribution function $g(x_1,x_2,v)$. How this is done is explained in the Appendix.

From (3.7) we can construct the following Monte Carlo algorthim.

(1) Find the subprocess type from the probabilities

$$P_m=\frac{\hat{h}_{m,\max}}{\sum_m\hat{h}_{m,\max}}$$

(the $\hat{h}_{m,\max}$ should be precalculated).

(2) Find the kinematical variables x_1, x_2, and v from the weighting distribution $g(x_1,x_2,v)dx_1dx_2dv$.

(3) Calculate the weight $\hat{h}_m(x_1,x_2,v)$.

(4) Accept or reject events by testing the ratio $R=\hat{h}_m/\hat{h}_{m,\max}$ (i.e., if $R<\xi$ go to step 1). (ξ is a random number uniformly distributed in 0.1.)

(5) Find the parton types which are involved in the hard scattering. For initial partons this is done according to the relative magnitude of the parton distributions at x and Q^2.

This algorithm allows the calculation of the single hard-scattering cross section $\sigma_{h,\mathrm{MC}}$ as

$$\sigma_{h,\mathrm{MC}}=\sum_m\sigma_{h,\mathrm{MC}}^m ,$$

where

$$\sigma_{h,\mathrm{MC}}^m=\frac{1}{N}\sum_{n=1}^{N}\hat{h}_m$$

is the cross section for a specified subprocess and N is the total number of rejected and accepted events for this subprocess.

The statistical error of the Monte Carlo calculation is found from

$$\Delta\sigma^m=\frac{1}{N}\left[\sum_{n=1}^{N}\hat{h}_m^2-\frac{1}{N}\left[\sum_{n=1}^{N}\hat{h}_m\right]^2\right]^{1/2}.$$

IV. RESULTS

In this section we present results obtained from the Monte Carlo event generator DTUJET-88.[11,12] All calculations use the parton distribution from MRS[23] set 1. The transverse-momentum cut $p_{\perp,\min}$ was set to 2 GeV/c and the hard scale was $Q^2=p_\perp^2/4$. For the minijets we have not included initial- and final-state bremsstrahlung effects to the hard-scattered partons. This will be done for events with higher transverse momentum. For the hadronization of chains, i.e., the transition of partons to hadrons, we use the independent fragmentation chain code BAMJET (Ref. 27) and the decay of resonances is handled by the code DECAY.[28]

In Fig. 5 the transverse-momentum distribution of charged particles as obtained by the model is compared with data obtained by the UA1 Collaboration[29] at the CERN Super Proton Synchrotron Collider at $\sqrt{s}=200$ and 900 GeV and by the CDF Collaboration[30] at the Fermilab collider at $\sqrt{s}=1800$ GeV. The curve according to the model reflects the two-component structure. In transverse-momentum regions where one component dominates—the soft component at $p_\perp<1$ GeV/c or the hard component at $p_\perp>2$ GeV/c—the data are well described, whereas in the range of 1–2 GeV/c the experimental data are underestimated. This is due to the fact that the transverse-momentum distribution of the partons at the end of the soft and hard chains does not match as qualitatively shown in Fig. 6. So there are too few partons with transverse momenta just below 2 GeV/c. A more smooth transition between the soft and hard parton $p_\perp$ distributions would result in more soft partons with higher transverse momentum and thus in more particles in the range 1–2 GeV/c. The average transverse-momentum results as shown in Fig. 7 also reflect this feature of the model. At higher energies the calculated average transverse momenta are too small compared to the experimental data.[29,30] This is due to the fact that the number of soft partons near 2 GeV/c is too small.

This problem can be solved by introducing empirically a p_t distribution for the partons at the ends of the soft sea chains, which at the cutoff transverse momentum of the hard chains joins continuously the p_t distribution of the partons at the ends of the hard chains. We use for the p_t distribution of the sea partons at the ends of the soft chains the simple parametrization

$$\frac{dN^{\text{soft sea}}}{2\pi p_t dp_t}=Ae^{Bp_t^2},\quad 0\le p_t\le p_{t,\text{cutoff}}\,. \tag{4.1}$$

The parameter A is determined from the normalization of (4.1) to the total number of partons at the soft sea-

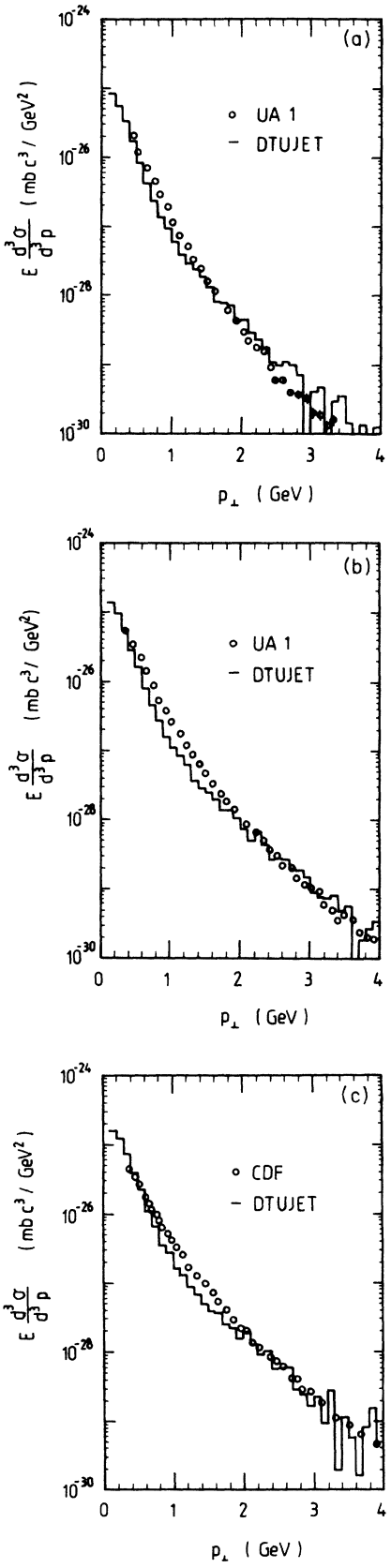

FIG. 5. Transverse-momentum distribution of charged particles compared with experimental data at $\sqrt{s}=200$, 900, and 1800 GeV (Refs. 29 and 30).

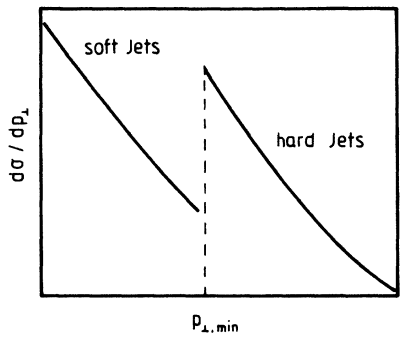

FIG. 6. Transverse-momentum distribution of the partons at the ends of soft and hard chains (qualitatively).

chain ends. The parameter B is determined from the continuity requirement

$$\frac{dN^{\text{soft sea}}}{2\pi p_t dp_t} = \frac{dN^{\text{hard}}}{2\pi p_t dp_t} \,. \tag{4.2}$$

We use $B = 1$ (GeV/c)^2.

The average transverse momenta obtained from this scheme are also given in Fig. 7 (crosses); the agreement to the experimental data is better than for the model with the discontinuity in the parton transverse-momentum distribution.

In Fig. 8 the rapidity plateau, i.e., the multiplicity of charged particles in the central region $\langle dn_{\text{ch}}/d\eta \rangle$ at $\eta = 0$ as a function of energy, is compared with experimental data.[29] This plateau does not depend on the transverse momentum of the partons and good agreement is obtained. Because of the logarithmic increase of both the plateau and the width of the rapidity distribution (see

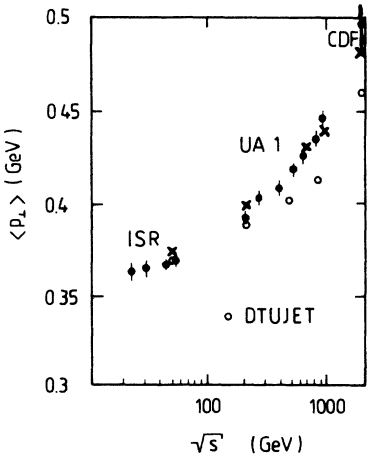

FIG. 7. Average transverse momentum per event over energy compared with experimental data. The open points give the DTUJET calculations with a discontinuous parton transverse-momentum distribution as given in Fig. 6. The crosses give the DTUJET calculations with a modified transverse-momentum distribution of the partons at the ends of the soft sea chains according to Eqs. (4.1) and (4.2).

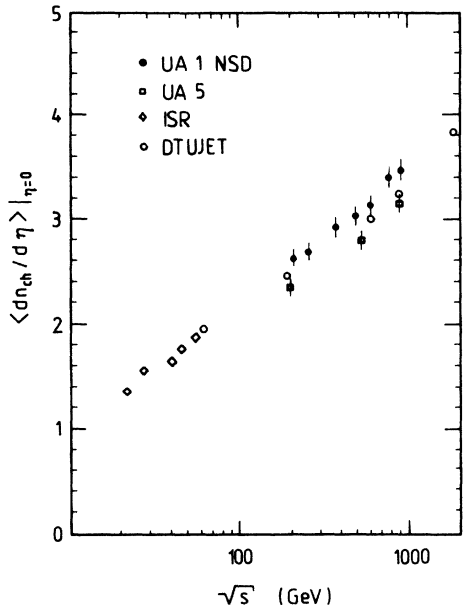

FIG. 8. Rapidity plateau $\langle dn_{\text{ch}}/d\eta \rangle$ at $\eta = 0$ for charged particles as a function of energy (Refs. 29 and 30).

Fig. 7 of Ranft *et al.*[10]) the model predicts a rise of the total multiplicity with energy proportional to $\ln^2 s$.

A rise of the plateau under the jets as determined by a jet-finding algorithm (the so-called pedestal effect), was found by the UA1 Collaboration at the CERN proton-antiproton collider.[7,31,32] Corresponding changes of the event structure predicted by our model when selecting subclasses of events with and without minijets were already presented by Ranft *et al.*[10] These changes follow as explained there from the changes in the Pomeron distributions (Fig. 4 of Ref. 10) between regions with $n_h = 0$ (n_h is the number of hard collisions in an event) and regions with $n_h > 0$.

We use here a jet-finding algorithm similar to the one used by the UA1 Collaboration[32] and calculate from the

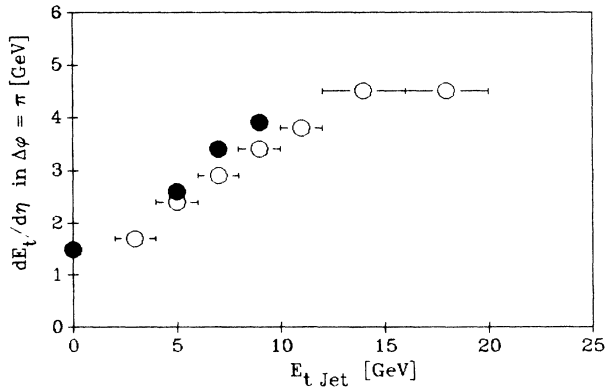

FIG. 9. Transverse-energy density $dE_t/d\eta$ in $\Delta\phi = \pi$ away from the jet axis (at $\Delta\eta = 1.5$) as a function of the jet transverse energy E_t. The open symbols give the UA1 data (Ref. 32). The solid points give the DTUJET calculations.

Monte Carlo events of the model the average transverse energy per pseudorapidity unit in average events and in the hemisphere opposite to the minijet in events with "jets" with transverse energies larger than 5, 7, and 9 GeV. In Fig. 9 we compare the rise of the transverse energy density $dE_t/d\eta$ in $\Delta\phi=\pi$ away from the jet axis at $\Delta\eta=1.5$ with the data of the UA1 Collaboration.[32] A good agreement is found. Because of the difficulties in getting in our Monte Carlo calculation as many events as analyzed by the UA1 Collaboration,[32] we calculate our $dE_t/d\eta$ for $E_{t,\text{jet}}$ larger than the given E_t values, while the experiment gives $dE_t/d\eta$ for events within narrow bins around the given E_t values. Therefore the $dE_t/d\eta$ values calculated from the model should be, as found in Fig. 9, somewhat larger than the experimental values.

ACKNOWLEDGMENTS

The model used here was formulated together with P. Aurenche, F. Bopp, A. Capella, J. Kwiecinski, P. Maire, and J. Tran Thanh Van, whom we thank for many discussions. One of the authors (J.R.) thanks Professor M. Tigner and Professor D. Groom for an invitation to the SSC central design group and Dr. K. Goebel and Dr. G. R. Stevenson for invitations to CERN. Parts of the calculations reported here were done at both laboratories.

APPENDIX

In this Appendix we will describe the sampling of x_1, x_2, and v from the weighting distribution

$$g_m(x_1,x_2,v)=\frac{\pi}{s}\frac{1}{(x_1x_2)^2}M_m^2\Theta(x_1x_2-a)\ . \tag{A1}$$

The way to do this depends on the subprocess m because of the different matrix elements M_m^2. We give here only an example for one process; the method for the other processes is similar and it is straightforward to transfer the algorithm. We describe the process $g+g\to g+g$ with the matrix element

$$M^2=\frac{9}{4}\left[3-uv-\frac{u}{v^2}-\frac{v}{u^2}\right]\ , \tag{A2}$$

where the symmetry factor $\frac{1}{2}$ is included.

For the purpose of selecting x_1, x_2, and v we can drop all constant factors and will do so from here on. Thus the distribution becomes

$$g(x_1,x_2,v)=\frac{1}{(x_1x_2)^2}\left[3-uv-\frac{u}{v^2}-\frac{v}{u^2}\right]\Theta(x_1x_2-a) \tag{A3}$$

with the allowed variable ranges given in (3.5).

Remembering that $u=-(1+v)$ one can see that g is symmetric in v with respect to $v=-\frac{1}{2}$ and that it is sufficient to take v from the interval $v_{\min}=-\frac{1}{2}$ to $v_{\max}=-\frac{1}{2}(1-W)$. Consequently, one has to exchange v and u with a probability of $\frac{1}{2}$ after the selection of v.

Now let us look for the singularity structure of g. The singularities are $1/x_i$ $(i=1,2)$ at $x_i\to a$ and $1/v^2$ at $v\to-\frac{1}{2}(1-W)$. We handle these singularities by introducing new variables which reflect the singularity structure.

For the v singularity we use

$$r=\frac{1}{v} \tag{A4}$$

with lower and upper limits

$$\begin{aligned} r_{\min}&=\frac{1}{v_{\max}}=\frac{1}{-\frac{1}{2}(1-W)}\ ,\\ r_{\max}&=\frac{1}{v_{\min}}=-2\ . \end{aligned} \tag{A5}$$

r is selected from

$$r=r_{\max}-\varphi_3(r_{\max}-r_{\min}) \tag{A6}$$

(φ_3 is a uniformly distributed random number in [0,1]).

With r as defined in (A4) we have, for the differentials,

$$\frac{dv}{v^2}=-d\left[\frac{1}{v}\right]=-dr=\frac{2W}{1-W}d\varphi_3\ . \tag{A7}$$

Using this and

$$1-W=\frac{1-W^2}{1+W}=\frac{a}{x_1x_2}\frac{1}{1+W} \tag{A8}$$

we get, for the weighting distribution,

$$\begin{aligned} g\,dx_1dx_2dv=&\left[3v^2-uv^3-u-\frac{v^3}{u^2}\right]W(1+W)\\ &\times\Theta(x_1x_2-a)d\varphi_3\frac{dx_1}{x_1}\frac{dx_2}{x_2}\ . \end{aligned} \tag{A9}$$

The remaining singularities are $1/x_1$ and $1/x_2$. Again we introduce a new variable z_i $(i=1,2)$ which is defined as

$$z_i=\ln(x_i)\ . \tag{A10}$$

The limits are

$$\begin{aligned} z_{i,\min}&=\ln(x_{i,\min})=\ln(a)\ ,\\ z_{i,\max}&=\ln(x_{i,\max})=\ln(1)=0\ , \end{aligned} \tag{A11}$$

and z_i is sampled from

$$\begin{aligned} z_i&=z_{i,\max}-\varphi_i(z_{i,\max}-z_{i,\min})\\ &=\ln(a)\varphi_i\ . \end{aligned} \tag{A12}$$

The Θ function written with the z_i becomes

$$\Theta(x_1x_2-a)=\Theta(z_1+z_2-\ln(a))\ . \tag{A13}$$

Putting things together we find

$$\begin{aligned} g\,dx_1dx_2dv=&\Theta(z_1+z_2-\ln(a))\left[3v^2-uv^3-u-\frac{v^2}{u^2}\right]\\ &\times W(1+W)d\varphi_1d\varphi_2d\varphi_3\ . \end{aligned} \tag{A14}$$

From this we have the following algorithm.
(1) Find $z_{1,2}=\ln(a)\varphi_{1,2}$.
(2) If $z_1+z_2<\ln(a)$ go to (1).
(3) Calculate $x_{1,2}=\exp(z_{1,2})$ and $W=(1-a/x_1x_2)^{1/2}$.
(4) Find $v=-0.5/[1+\varphi_3 W/(1-W)]$.
(5) Calculate the remaining weight

$$w=W(1+W)\left[3v^2-uv^3-u-\frac{v^3}{u^2}\right]$$

and reject [go to (1)] if $w_{\max}<\varphi_4$.
(6) If $\varphi_5<\frac{1}{2}$ set $v=-(1+v)$.

[1]A. Capella, U. Sukhatme, C.-I. Tan, and J. Tran Thanh Van, Phys. Lett. **81B**, 68 (1979); Z. Phys. C **3**, 329 (1979); A. Capella and J. Tran Thanh Van, *ibid.* **10**, 249 (1981); Phys. Lett. **114B**, 450 (1982).

[2]P. Aurenche and F. W. Bopp, Z. Phys. C **13**, 205 (1982); Phys. Lett. **114B**, 363 (1982).

[3]A. B. Kaidalov, Phys. Lett. **116B**, 459 (1982); A. B. Kaidalov and K. A. Ter-Martirosyan, *ibid.* **117B**, 247 (1982).

[4]J. Ranft, P. Aurenche, and F. W. Bopp, Z. Phys. C **26**, 279 (1984); P. Aurenche, F. W. Bopp, and J. Ranft, *ibid.* **23**, 67 (1984).

[5]P. Aurenche, F. W. Bopp, and J. Ranft, Phys. Rev. D **33**, 1867 (1986).

[6]UA1 Collaboration, G. Arnison *et al.*, Phys. Lett. **118B**, 167 (1982).

[7]UA1 Collaboration, C.-E. Wulz, Report No. CERN-EP/87-84, 1987 (unpublished).

[8]A. Capella, J. Tran Thanh Van, and J. Kwiecinski, Phys. Rev. Lett. **58**, 2015 (1987).

[9]L. Durand and H. Pi, Phys. Rev. Lett. **58**, 303 (1987).

[10]J. Ranft, P. Aurenche, F. Bopp, A. Capella, K. Hahn, J. Kwiecinski, P. Maire, and J. Tran Thanh Van, Report No. SSC-149, 1987 (unpublished).

[11]J. Ranft, Report No. SSC-150, 1987 (unpublished).

[12]J. Ranft and K. Hahn, CERN Report No. TIS-RP/218, 1988 (unpublished).

[13]J. Ranft and S. Ritter, Z. Phys. C **20**, 347 (1983); **24**, 569 (1985).

[14]J. Ranft, Phys. Rev. D **37**, 1842 (1988).

[15]Y. Iga, R. Hamatsu, S. Yamazaki, and H. Sumiyashi, Z. Phys. C **38**, 557 (1988).

[16]K. Werner, in *Quark Matter,* proceedings of Quark Matter 1987: 6th International Conference on Ultrarelativistic Nucleus-Nucleus Collisions, Schloss Nordkirchen, Germany, 1987, edited by H. Satz, H. J. Specht, and R. Stock (Springer, Berlin, 1988); K. Werner and M. Kutchera, Phys. Lett. B **183**, 385 (1987).

[17]J. P. Pansart, in *Proceedings of the 5th International Conference on Ultra Relativistic Nucleus-Nucleus Collisions,* Pacific Grove, California, 1986, edited by L. S. Schroeder and M. Gyulassy [Nucl. Phys. **A461** (1987)].

[18]V. A. Abramovski, V. N. Gribov, and O. V. Kanchelli, Yad. Phys. **18**, 595 (1974) [Sov. J. Nucl. Phys. **18**, 308 (1974)].

[19]L. V. Gribov, E. M. Levin, and M. G. Ryskin, Phys. Rep. **100**, 1 (1983).

[20]A. H. Mueller and J. Qiu, Nucl. Phys. **B268**, 427 (1986).

[21]J. C. Collins, Illinois Tech. Report No. 86-0298, 1986 (unpublished).

[22]E. Eichten, I. Hinchliffe, K. Lane, and C. Quigg, Rev. Mod. Phys. **56**, 579 (1984); **58**, 1065 (1986).

[23]A. D. Martin, R. G. Roberts, and W. J. Stirling, Phys. Rev. D **37**, 1161 (1988).

[24]F. E. Paige and S. D. Protopopescu, in *Physics of the Superconducting Super Collider, Snowmass, 1986,* proceedings of the Summer Study, Snowmass, Colorado, 1986, edited by R. Donaldson and J. Marx (Division of Particles and Fields of the APS, New York, 1987), p. 320.

[25]H. U. Bengtson and T. Sjoestrand, Comput. Phys. Commun. **46**, 43 (1987).

[26]B. L. Combridge, J. Kripfganz, and J. Ranft, Phys. Lett. **70B**, 234 (1977).

[27]S. Ritter and J. Ranft, Acta Phys. Polonica B **11**, 259 (1980); S. Ritter, Z. Phys. C **6**, 27 (1982); Comput. Phys. Commun. **31**, 393 (1984).

[28]K. Hänssgen and S. Ritter, Comput. Phys. Commun. **31**, 411 (1984).

[29]UA1 Collaboration, S. J. Wimpenny *et al.*, University of California Report (Riverside) No. UCR/EXP 88-105, 1988 (unpublished).

[30]CDF Collaboration, F. Abe *et al.*, Phys. Rev. Lett. **61**, 1819 (1988).

[31]UA1 Collaboration presented by F. Ceradini, in *Proceedings of the International Europhysics Conference of High Energy Physics,* Bari, Italy, 1985, edited by L. Nitti and G. Preparata (Laterza, Bari, 1985).

[32]UA1 Collaboration, C. Albajar *et al.*, Nucl. Phys. **B309**, 405 (1988).